Probing the chirality structure in the lepton-flavor-violating Higgs decay $h \to \tau\mu$ at the LHC

Mayumi Aoki,[1,*] Shinya Kanemura,[2,†] Michihisa Takeuchi,[3,4,‡] and Lalu Zamakhsyari[1,§]

[1]*Institute for Theoretical Physics, Kanazawa University, Kanazawa 920-1192, Japan*
[2]*Department of Physics, Osaka University, Toyonaka, Osaka 560-0043, Japan*
[3]*School of Physics and Astronomy, Sun Yat-sen University, 519082 Zhuhai, China*
[4]*Graduate School of Information Science and Technology, Osaka University, Suita, Osaka 565-0871, Japan*

(Received 5 January 2023; accepted 24 February 2023; published 24 March 2023)

A phenomenological study for determining the chirality structure in lepton-flavor-violating Higgs decays $h \to \tau\mu$ at the LHC is presented. We estimate the effects of the τ polarization in the analysis and the importance of determining the relative visible momentum ratio x, and show the analysis with a collinear mass m_{col1} by assuming one missing particle is appropriate. We find that the sensitivity would be generically affected up to ± 4–6% in terms of the $\mathrm{BR}(h \to \tau\mu)$ upper bound, and show the altered bounds on the $(|y_{\mu\tau}|, |y_{\tau\mu}|)$ plane. We further study the benchmark scenarios, and demonstrate the sensitivity study for the chirality structure using the relative visible momentum ratio. We find that the two fully polarized cases, the τ_R and τ_L scenarios consistent with the recently reported excess, are distinguishable at 2σ level for 1000 fb^{-1}. We also show that a further improved study potentially provides a similar sensitivity already for 139 fb^{-1}.

DOI: 10.1103/PhysRevD.107.055037

I. INTRODUCTION

The discovery of 125 GeV Higgs boson [1,2] is certainly one of the most important discoveries in particle physics. It has been proven so far that properties of the Higgs boson are consistent with the standard model (SM) predictions. However, the present data do not rule out possibilities of new mechanisms of electroweak symmetry breaking or new electroweak physics beyond the SM. The effects of such new physics would modify the couplings of the 125 GeV Higgs boson from the SM predictions or introduce new interactions that are absent in the SM. An example of the latter is the lepton-flavor-violating Higgs (HLFV) processes, which involve introduction of off-diagonal components of the Yukawa coupling y_{ij} for the lepton sector in the effective Lagrangian term:

$$-\mathcal{L}_{hll} = y_{ij}\bar{l}_{Li}hl_{Rj} + \mathrm{H.c.}, \tag{1}$$

where the HLFV couplings are induced at the tree level or as the loop effect. The two Higgs doublet models (2HDMs), for instance, induce the HLFV couplings at the tree level [3–14], meanwhile the seesaw models [15–21] and minimal supersymmetric standard models [3,16,22–34] at the one-loop level.

The off-diagonal components are responsible for HLFV decays, $h \to l_i l_j$ $(i \neq j)$, where $h \to l_i l_j$ mean the sum of the processes $h \to l_i^+ l_j^-$ and $h \to l_i^- l_j^+$. Any observation of HLFV decays is a clear evidence of new physics beyond the SM. The prospects of probing HLFV decays at the LHC and future colliders have been widely explored in a model independent way [3,35–43] and in the various models [3–34,44–69].

Among $h \to l_i l_j$ processes, the $h \to \mu e$ is strongly suppressed due to the stringent constraint on $y_{\mu e}$ from the rare μ decay [70]. On the other hand, the $h \to \tau e$ and $h \to \tau\mu$ are less constrained. In this paper, we focus on $h \to \tau\mu$ since we would expect naturally larger effects and also $h \to \tau e$ is known to be experimentally more challenging. The relevant Yukawa coupling $y_{\tau\mu}$ is also constrained by the low-energy LFV processes, where the strongest one is coming from $\tau \to \mu\gamma$. However, those constraints are still weaker than the current bounds in the HLFV decays by the ATLAS [71,72] and CMS [73] collaborations. Even with the future $\tau \to \mu\gamma$ measurement at Belle II [74], the constraints on $y_{\tau\mu}$ from the HLFV decays will still be the most stringent. Current measurements of branching ratios (BRs) of the HLFV decays $h \to l_i l_j$ at the LHC give the constraints on

*mayumi.aoki@staff.kanazawa-u.ac.jp
†kanemu@het.phys.sci.osaka-u.ac.jp
‡takeuchi@mail.sysu.edu.cn
§lalu_zamakhsyari@stu.kanazawa-u.ac.jp

$\bar{y}_{ij} \equiv \sqrt{|y_{ij}|^2 + |y_{ji}|^2}$. At the future hadron and lepton colliders, we expect to improve the limit on $\bar{y}_{\tau\mu}$ and also to probe the chirality structure of the Yukawa matrix, for example, the ratio $y_{\tau\mu}/y_{\mu\tau}$ through the measurements in the HLFV decays.[1] Therefore, the way to probe the chirality structure in the leptonic Yukawa sector would play an important role in distinguishing the models if such processes are observed.

In this paper, we study the HLFV decay $h \to \tau\mu$ at the LHC, and study the chirality structure of the process in the SMEFT. The numbers of signal events for $h \to \tau_L \mu_R$ and $h \to \tau_R \mu_L$, and those of backgrounds are evaluated. We focus on the gluon fusion (GGF) Higgs boson production in the simulation as a main production mode and hadronic τ decay modes are considered. We show that the collinear mass based on one missing particle assumption is important for getting the better discrimination sensitivity between $h \to \tau_L \mu_R$ and $h \to \tau_R \mu_L$. We show the resulting sensitivity on the off-diagonal elements of the Yukawa coupling matrix, and express it in the $(|y_{\tau\mu}|, |y_{\mu\tau}|)$ plane.

This paper is organized as follows. In Sec. II, we summarize the current constraints on the $\mu - \tau$ sector. Theoretical frameworks of the HLFV for new physics beyond the SM are described in Sec. III. In Sec. IV, we discuss the collider simulation of the HLFV process $h \to \tau\mu$ taking the polarization effects of τ lepton into account, and present the results on the upper limit of the BR of $h \to \tau\mu$, and the corresponding HLFV Yukawa couplings $y_{\tau\mu}$ and $y_{\mu\tau}$. We also consider the three benchmark scenarios with different chirality structures, which are inspired by the recent excess reported by ATLAS, and demonstrate the way to discriminate the scenarios. Section V is devoted to the discussion and summary.

II. EXPERIMENTAL STATUS

The ATLAS and CMS have searched for $h \to l_i l_j$ and provide the upper bounds on those BRs. For our interest in HLFV $h \to \tau\mu$, the upper limit on the BR$(h \to \tau\mu)$ at 95% C.L. is reported as [71,73]

$$\mathrm{BR}(h \to \tau\mu) \leq 0.28\% \ (\mathrm{ATLAS}) \quad \text{and} \quad 0.15\% \ (\mathrm{CMS}), \tag{2}$$

at the total integrated luminosity of 36.1 and 139 fb^{-1}, respectively.[2] These limits are interpreted as $\sqrt{|y_{\mu\tau}|^2 + |y_{\tau\mu}|^2} < 1.5 \times 10^{-3}$ (ATLAS) and 1.11×10^{-3} (CMS), respectively.

[1]There are models to predict such an asymmetry. See, e.g., [75–79].

[2]Recently, the ATLAS collaboration gives the bound BR$(h \to \tau\mu) < 0.18\%$, which is obtained from the combined searches in $\mu\tau$ and $e\tau$ channels with 138 fb^{-1}, and exhibits 2.2σ level upward deviation in comparison with the expected sensitivity 0.09% [72].

TABLE I. Current experimental bounds and future sensitivities for several low-energy LFV observables in the $\tau - \mu$ sector.

LFV process	Present bound BR	Future sensitivity
$\tau \to \mu\gamma$	4.4×10^{-8} [81]	$\sim 10^{-9}$ [74]
$\tau \to \mu\mu\mu$	2.1×10^{-8} [89]	5×10^{-10} [74]
$\tau^- \to e^-\mu^+\mu^-$	2.7×10^{-8} [89]	5×10^{-10} [74]
$\tau^- \to \mu^- e^+ e^-$	1.8×10^{-8} [89]	5×10^{-10} [74]
$\tau^- \to e^+\mu^-\mu^-$	1.7×10^{-8} [89]	4×10^{-10} [74]
$\tau^- \to \mu^+ e^- e^-$	1.5×10^{-8} [89]	3×10^{-10} [74]

The projected limit at the high luminosity LHC (3000 fb^{-1}) has been estimated at $\sim 10^{-4}$ [42,43]. Furthermore, the HLFV decay would also be searched for in the future e^+e^- colliders, where the sensitivity for the HLFV branching ratios would also reach $\sim 10^{-4}$ as shown by several analyses [4,41,55,61,80].

The LFV Yukawa couplings relevant to the $h \to l_i l_j$ process also induce the low-level LFV processes, such as $l_i \to l_j\gamma$ and $l_i \to l_j l_k l_k$ processes. The bounds for the relevant low-level LFV processes in the τ-μ sector are given in Table I. Although they are all around $\sim 10^{-8}$, the $\tau \to \mu\gamma$ measurement provides the strongest bound, $\sqrt{|y_{\mu\tau}|^2 + |y_{\tau\mu}|^2} < 0.016$ [38,81]. This bound is still weaker than the current bound from the HLFV decay process of $h \to \tau\mu$. All future sensitivities are promised to increase up to one or two orders of magnitude as summarized in Table I. The HLFV couplings of $y_{\mu\tau}$ and $y_{\tau\mu}$ are also constrained from the measurements of the anomalous magnetic moment $(g-2)_\mu$ [82], the muon electric dipole moment [83], the tau electric dipole moment [84,85], as well as the lepton-nucleus scattering $\mu N \to \tau X$ [86–88], whereas they are weaker than the constraints from $\tau \to \mu\gamma$.

III. THEORETICAL FRAMEWORK FOR THE HLFV PROCESS

We here briefly introduce the HLFV couplings in a model-independent manner following the effective-field theory extension of the SM (SMEFT). This is well motivated in the current situation with the absence of new physics signatures at the LHC, which supports any new particles responsible for a new physics would be well beyond the current electroweak scale. The type III 2HDM is also introduced as an example concrete model which induces the HLFV couplings at tree level.

A. Standard model effective-field theory

The general form of the SMEFT is given by

$$\mathcal{L}_{\mathrm{EFT}} = \mathcal{L}^{(4)}_{\mathrm{SM}} + \frac{1}{\Lambda}\sum_a C^{(5)}_a Q^{(5)}_a + \frac{1}{\Lambda^2}\sum_a C^{(6)}_a Q^{(6)}_a + \mathcal{O}\left(\frac{1}{\Lambda^3}\right), \tag{3}$$

where Λ is the NP scale, $Q_a^{(d)}$ are the d-dimension operators composed of the SM fields, and their associated Wilson coefficients $C_a^{(d)}$ are in general complex (flavor indices have been suppressed). The dimension-five operator is the Weinberg operator that gives rise to the neutrino Majorana mass [90], so this is not our concern. The higher dimension $d > 6$ contributions are suppressed for HLFV, so that our main focus for HLFV is the dimension-six operators. The operator $Q_a^{(6)}$ is usually presented in the Warsaw basis [90,91], and the one that is relevant for HLFV is given by

$$Q^{l\varphi} = (\varphi^\dagger\varphi)\bar{L}'_L C^{l\varphi} l'_R \varphi, \tag{4}$$

where L'_L and l'_R are the lepton $\mathrm{SU}(2)_L$ doublet and singlet, respectively, in flavor space, and φ is the $\mathrm{SU}(2)_L$ Higgs doublet. Other dimension-six Warsaw operators that induce the HLFV couplings are suppressed, or can be reduced to Eq. (4) via field redefinitions, Fierz identities, and equations of motions [58].

After the electroweak symmetry breaking, the lepton Yukawa Lagrangian in the SM, $-\mathcal{L}_Y^{\mathrm{SM}} = \bar{L}'_L Y^l l'_R \varphi + \mathrm{H.c.}$., where Y^l is the Yukawa matrix, and the effective low energy Lagrangian by the operator $Q^{l\varphi}$, $\mathcal{L}_{\mathrm{HLFV}}$, can be written as

$$-(\mathcal{L}_Y^{\mathrm{SM}} + \mathcal{L}_{\mathrm{HLFV}}) = \bar{l}'_L \left[\frac{v}{\sqrt{2}}\left(Y^l - \frac{C^{l\varphi}v^2}{2\Lambda^2}\right) + \frac{h}{\sqrt{2}}\left(Y^l - \frac{3C^{l\varphi}v^2}{2\Lambda^2}\right)\right] l'_R + \mathrm{H.c.}, \tag{5}$$

where the first and second terms cannot be diagonalized simultaneously. Rotating the lepton into mass state,

$$l'_L = V_L l_L, \qquad l'_R = V_R l_R, \tag{6}$$

we obtain the Yukawa coupling matrix for $\mathcal{L}_{hll}$ in Eq. (1) as

$$y_{ij} = \frac{m_{ij}}{v}\delta_{ij} - \frac{v^2}{\sqrt{2}\Lambda^2}(V_L^\dagger C^{l\varphi} V_R)_{ij}, \tag{7}$$

which is an arbitrary nondiagonal matrix. The off-diagonal elements in Eq. (7) lead to the HLFV decays $h \to l_i l_j$ with branching ratios given by

$$\mathrm{BR}(h \to l_i l_j) = \frac{m_h}{8\pi\Gamma_h}|\bar{y}_{ij}|^2, \qquad \bar{y}_{ij} \equiv \sqrt{|y_{ij}|^2 + |y_{ji}|^2}, \tag{8}$$

where $m_h = 125$ GeV is the SM Higgs boson mass, and $\Gamma_h \simeq 4.1$ MeV is the total SM Higgs boson decay width. When the chiral interactions are written explicitly for $\mathrm{BR}(h \to \tau\mu)$, we obtain

$$\mathrm{BR}(h \to \tau_L \mu_R) = \frac{m_h}{8\pi\Gamma_h}|y_{\tau\mu}|^2,$$
$$\mathrm{BR}(h \to \mu_L \tau_R) = \frac{m_h}{8\pi\Gamma_h}|y_{\mu\tau}|^2. \tag{9}$$

B. Two Higgs doublet model

The 2HDM is a model with an extension of a electroweak scalar doublet. If there is no discrete symmetry that prevents the flavor changing neutral current is introduced, then the Yukawa matrices can no longer be simultaneously diagonalized so flavor-violating interactions are appeared at the tree level. Assuming CP conservation, the 2HDM provides four more additional scalars, i.e., the CP-even neutral Higgs boson H, the CP-odd neutral Higgs boson A and the charged Higgs bosons $H^\pm$ beside the SM-like Higgs boson h.

In the Higgs basis, H_1 and H_2 can be parametrized as

$$H_1 = \begin{pmatrix} G^+ \\ \frac{1}{\sqrt{2}}(v + \varphi_1 + iG^0) \end{pmatrix}, \quad H_2 = \begin{pmatrix} H^+ \\ \frac{1}{\sqrt{2}}(\varphi_2 + iA) \end{pmatrix}, \tag{10}$$

where G^+ and G^0 are the Nambu-Goldstone bosons.

The CP-even neutral components φ_1 and φ_2 can be rotated to the mass eigenstates h and H by an orthogonal rotation with the mixing angle $\theta_{\beta\alpha}$ as

$$\begin{pmatrix} \varphi_1 \\ \varphi_2 \end{pmatrix} = \begin{pmatrix} \cos\theta_{\beta\alpha} & \sin\theta_{\beta\alpha} \\ -\sin\theta_{\beta\alpha} & \cos\theta_{\beta\alpha} \end{pmatrix} \begin{pmatrix} H \\ h \end{pmatrix}. \tag{11}$$

Note that h is the SM-like Higgs boson for $\sin\theta_{\beta\alpha} \simeq 1$.

The lepton Yukawa sector is given by

$$-\mathcal{L}_Y^{\mathrm{2HDM}} = \bar{L}'_L Y_1 l'_R H_1 + \bar{L}'_L Y_2 l'_R H_2 + \mathrm{H.c.}, \tag{12}$$

where Y_1 and Y_2 are the Yukawa matrices. The relevant terms to the HLFV decays after the electroweak symmetry breaking are given as

$$-\mathcal{L}_Y^{\mathrm{2HDM}} \supset \bar{l}'_L \frac{vY_1}{\sqrt{2}} l'_R + \bar{l}'_L \left(\frac{Y_1}{\sqrt{2}}\sin\theta_{\beta\alpha} + \frac{Y_2}{\sqrt{2}}\cos\theta_{\beta\alpha}\right)\bar{l}'_R h + \mathrm{H.c.} \tag{13}$$

Rotating the leptons into their mass basis, we obtain

$$-\mathcal{L}_Y^{\mathrm{2HDM}} \supset \bar{l}_{L,i}(m_{ij}\delta_{ij}) l_{R,j} + \bar{l}_{L,i}\left[\frac{m_{ij}\delta_{ij}}{v}\sin\theta_{\beta\alpha} + \frac{\cos\theta_{\beta\alpha}}{\sqrt{2}}\xi_{ij}\right] l_{R,j} h + \mathrm{H.c.}, \tag{14}$$

where m is the diagonal lepton mass matrix,

$$m_{ij} = \frac{v(V_L^\dagger Y_1 V_R)_{ij}}{\sqrt{2}} = \mathrm{diag}(m_e, m_\mu, m_\tau)_{ij}, \tag{15}$$

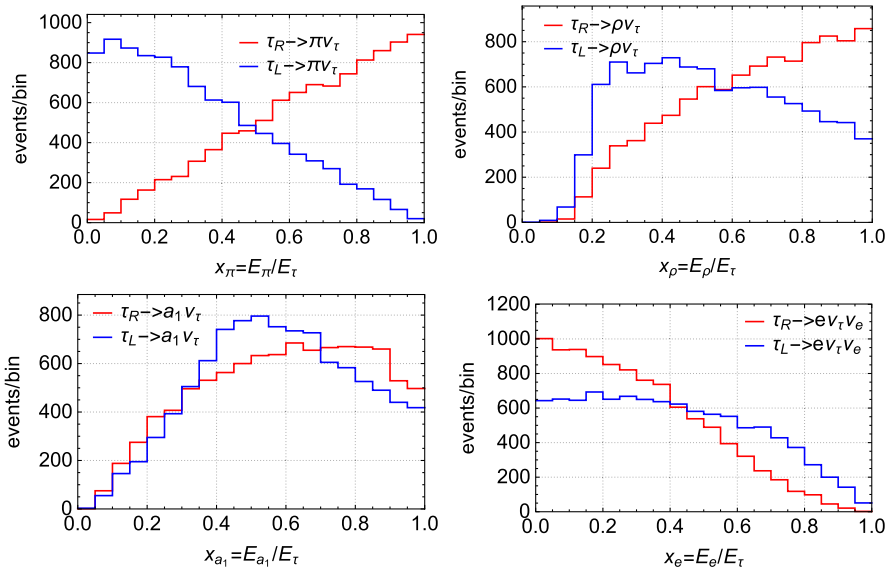

FIG. 1. The distribution of energy fraction of π, ρ, a_1 (hadronic) and e (leptonic), i.e., x_π, x_ρ, x_{a_1} as the decay product of τ leptons for different polarizations at the parton level.

and $\xi_{ij} \equiv (V_L^\dagger Y_2 V_R)_{ij}$, which is generally a nondiagonal matrix. The second term in Eq. (14) corresponds to $\mathcal{L}_{hll}$ in Eq. (1), and BRs of the HLFV decays are given by[3]

$$\mathrm{BR}(h \to l_i l_j) = \frac{m_h \cos^2\theta_{\beta\alpha}}{16\pi\Gamma_h}|\bar{\xi}_{ij}|^2, \quad \bar{\xi}_{ij} = \sqrt{|\xi_{ij}|^2 + |\xi_{ji}|^2}. \tag{16}$$

The BRs for chiral processes are given by

$$\mathrm{BR}(h \to \tau_L \mu_R) = \frac{m_h \cos^2\theta_{\beta\alpha}}{16\pi\Gamma_h}|\xi_{\tau\mu}|^2,$$
$$\mathrm{BR}(h \to \mu_L \tau_R) = \frac{m_h \cos^2\theta_{\beta\alpha}}{16\pi\Gamma_h}|\xi_{\mu\tau}|^2. \tag{17}$$

IV. ANALYSIS AT THE LHC

A. Polarized taus

At the LHC, constraints on the HLFV couplings $y_{\tau\mu}$ and $y_{\mu\tau}$ are obtained by interpreting the search results of $h \to \tau\mu$ process. In principle, the current studies should already be sensitive to the chirality structure. To understand that, let us summarize the properties of the τ decays. We mainly focus on the case that the τ leptons decay hadronically $\tau \to$ hadrons $+ \nu_\tau$ in the $h \to \tau\mu$ events, that is

$$pp \to h \to \tau^\pm \mu^\mp \to \tau_h^\pm + \nu_\tau + \mu^\mp. \tag{18}$$

[3]The other terms in Eq. (14) induce other LFV Higgs boson decays $H \to l_i l_j$ and $A \to l_i l_j$ [43,92–95].

Here and in the following, we denote the visible components of the hadrons as τ_h, which is expected to be identified as a τ-tagged jet at the collider experiment. In addition to the leptonic decay contributions from the $e\nu$ (17.8%) and $\mu\nu$ (17.4%) modes, main hadronic decay modes of the τ leptons are categorized into the following three groups:

(1) $\pi^\pm$ mode (9.3%): $\tau^\pm \to \pi^\pm \nu_\tau$,
(2) $\rho^\pm$ mode (25.5%): $\tau^\pm \to \rho^\pm \nu_\tau \to \pi^\pm \pi^0 \nu_\tau$,
(3) $a_1^\pm$ mode (27%): $\tau^\pm \to a_1^\pm \nu_\tau \to \pi^\pm \pi^0 \pi^0 \nu_\tau / \pi^\pm \pi^\pm \pi^\mp \nu_\tau$.

All three mesons π, ρ, and a_1 are found in a one-prong mode, but in principle we can distinguish them by the number of neutral pions, meanwhile a_1 is also found in a three-prong mode. In the all hadronic decay modes, these contributions are 98%. Thus, we consider only these modes.

These hadronic decay modes carry the information on the polarization of τ leptons [96,97], i.e. whether τ_L or τ_R. One of such simple observables is the fractional energy of τ decay products $x_i = E_i/E_\tau$ $(i = \pi, \rho, a_1, e)$. Figure 1 shows the simulated x_i distributions at the parton level for a τ_L (left-handed τ lepton), and for a τ_R (right-handed τ lepton), which are realized by fixing $(y_{\mu\tau}, y_{\tau\mu}) = (0, 1)$ and $(y_{\mu\tau}, y_{\tau\mu}) = (1, 0)$ in our effective model, respectively. The polarized τ decays is simulated by the package TAUDECAY [97]. In fact these results are consistent with the fractional energy distributions of τ lepton [96,98]. Among four decay modes shown in Fig. 1, the effect on τ polarization is most prominent in the $\pi^\pm$ modes. The x_π distribution is hard for τ_R while it is soft for τ_L. For the ρ and a_1 modes, x_ρ and x_{a_1} are relatively high for both $\tau_{L/R}$ cases, and again they are harder for τ_R than those for τ_L although they are less sensitive to the polarization. On the other hand, the e-modes provide relatively softer x_e distributions due to the existence of an additional neutrino,

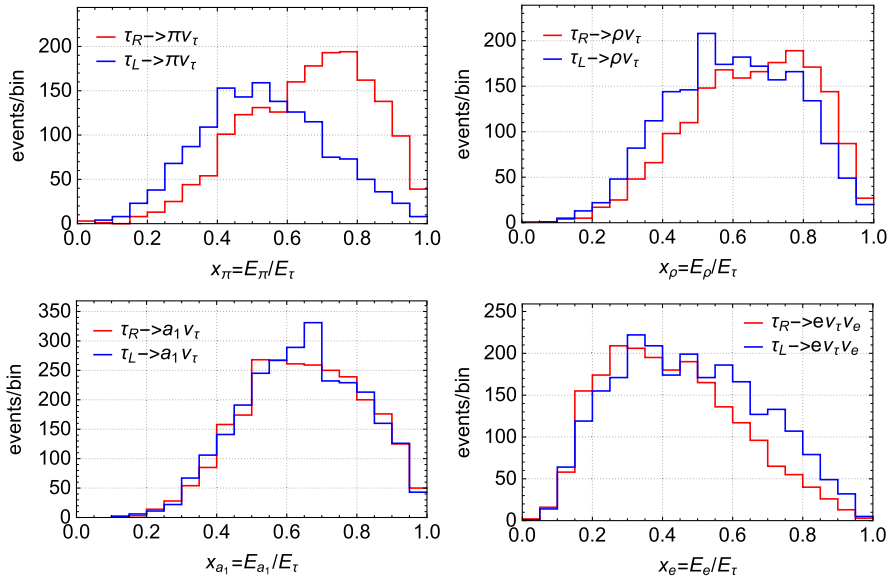

FIG. 2. The distribution of energy fraction of π, ρ, a_1 (hadronic) and e (leptonic) as decay product of τ leptons for different polarization at detector level.

and harder x_e distribution is obtained for τ_L than that for τ_R oppositely to the other hadronic modes.

Figure 2 shows the corresponding x_i distributions at the reconstructed jet level after the detector simulation. Although they are smeared, the tendencies discussed above are still visible. For the jet level observables, we see a significant reduction in lower region of x_i both for τ_L and τ_R. This is due to the effects of the jet energy threshold, and the events falling down below it cannot be observed. Therefore, the polarization affects the acceptance of the events even though the normalized distributions look similar.

In our analysis, since $\mathrm{BR}(h \to \mu_L \tau_R) \propto |y_{\mu\tau}|^2$, $\mathrm{BR}(h \to \tau_L \mu_R) \propto |y_{\tau\mu}|^2$ and both can be considered as the independent processes if we neglect the spin correlation effects, any distributions can be expressed as

$$f(x; y_{\mu\tau}, y_{\tau\mu}) = |y_{\mu\tau}|^2 f_R(x) + |y_{\tau\mu}|^2 f_L(x). \quad (19)$$

Therefore, we discuss the fully polarized cases in this paper: $(y_{\mu\tau}, y_{\tau\mu}) = (1, 0)$ and (0,1), corresponding to the decays into $\tau_R \mu_L$ and $\tau_L \mu_R$, respectively. We obtain the results for any general case in the $(y_{\mu\tau}, y_{\tau\mu})$ plane by using the above relationship.

B. Simulation

In this section we would like to show how much τ polarization effects described above affect the results. Our study is based on the ATLAS study at 36.1 fb^{-1} [71]. We also would like to propose an improved analysis strategy aiming for identifying the HLFV process $h \to \tau\mu$. After performing the collider simulation, we show that the sensitivity in the $(y_{\mu\tau}, y_{\tau\mu})$ plane by the $h \to \tau\mu$ process should be asymmetric due to the τ polarization effects.

Although we would like to directly follow the ATLAS analysis, since they provide a results heavily based on the BDT results, we try to roughly reproduce their results, and discuss the τ polarization effects based on our simulation. They show that at current statistics of 36.1 fb^{-1}, the most relevant production modes are still the GGF process since the vector boson fusion (VBF) modes are statistically still limited. Thus in this paper, we focus on the gluon fusion production mode. For the final states we focus on the $\tau_h\mu$ channel, since it provides the strongest sensitivity on the HLFV coupling among the relevant channels, which include $\mu\tau_e$ and the corresponding VBF channels. There are many different SM backgrounds for the HLFV signal but we only consider the most dominant SM background Z + jets followed by the decay $Z \to \tau^+\tau^-$, which in the end contribute about a half of the SMBGs as shown in ATLAS [71] and CMS [73].

We generate signal and background events with MG5_aMC@NLO [99] at leading order with $\sqrt{s} = 13$ TeV. The parton shower, hadronization, and the detector response are simulated by PYTHIA8 [100] and DELPHES [101] with the default ATLAS detector card. The HLFV signal $h \to \tau\mu$ is generated using the 2HDM where we translated the LFV Yukawa couplings of EFT to the 2HDM term via Eq. (17) fixing the mixing angle $\cos\theta_{\beta\alpha} = 0.1$. In the following, we show the two cases $(y_{\mu\tau}, y_{\tau\mu}) \propto (0, 1)$ and (1,0) for the benchmarks, corresponding to the τ_R and τ_L cases, respectively, and mainly show the numbers for the case of $\mathrm{BR}(h \to \tau\mu) = 1\%$. We scale the normalization of the signal samples to reproduce the total GGF Higgs production cross section of 48.6 pb, which is the next-to-next-to-next-to-leading order ($\mathrm{N^3LO}$)

TABLE II. Baseline event selection cuts applied for the $\tau_h\mu$ channels.

	Selection cuts
Baseline	Exactly 1μ and 1τ jet (opposite sign) $p_{T,\mu} > 27.3$ GeV, $p_{T,\tau_{\rm vis}} > 25$ GeV $\lvert\Delta\eta(\mu,\tau_{\rm vis})\rvert < 2.0$ $\sum_{i=l,\tau_{\rm vis}} \cos\Delta\phi(i,\not{E}_T) > -0.35$

GGF Higgs production cross section at 13 TeV. Numerically, ignoring the correction to the Higgs total width, we adopt the following relation including the QCD and the other corrections [102–105],

$$\mathrm{BR}(h\to\tau\mu) = 0.12\% \times \frac{(|y_{\mu\tau}|^2 + |y_{\tau\mu}|^2)}{10^{-6}}. \tag{20}$$

For example, numerically, $\bar{y}_{\mu\tau} = m_\tau/v \simeq 0.0072$ corresponds to $\mathrm{BR}(h\to\tau\mu) = 6.3\%$.

For the GGF $\tau_h\mu$ channel, or non-VBF $\tau_h\mu$ channel, we require the following baseline cuts: exactly one isolated muon and exactly one τ jet are required, and their charges are opposite each other. We rely on DELPHES for τ-jet identification and we select the working point of the tagging efficiency of 60%. Furthermore, an upper limit on the pseudorapidity difference between μ and τ jet, $|\Delta\eta(\mu,\tau_{\rm vis})| < 2.0$ is applied to reduce the background from misidentified τ candidates [71]. To avoid the missing momentum coming from other sources, the sum of the cosine of the angle between $\mu(\tau_{\rm vis})$ and missing momentum in transverse plane is large enough, $\sum_{i=l,\tau_{\rm vis}} \cos\Delta\phi(i,\not{E}_T) > -0.35$. The baseline cut is summarized in Table II. For the signal samples, we generate 500 000 events per each τ_R, τ_L sample, while 1 000 000 events are generated for $Z\to\tau\tau$ background.

C. Analysis with collinear masses

1. Collinear mass for two missing particles $m_{\rm col2}$

The conventional analyses on $h\to\tau\mu$ in literature often follow the analyses motivated for the reconstruction of $h\to\tau\tau$ events. Thus, the most studies rely on the reconstructed invariant mass $m_{\tau\tau}$ using the so-called collinear approximation, $m_{\rm col}$ [71,106], which we explicitly denote $m_{\rm col2}$ in this paper. The collinear approximation is based on the assumption that the momentum of the all invisible decay products of a τ lepton $\boldsymbol{p}_\tau^{\rm invis}$ and the momentum of the all visible decay products of a τ lepton $\boldsymbol{p}_\tau^{\rm vis}$ are in parallel to the original τ momentum, that is, we can express with the real parameter x as

$$\boldsymbol{p}_\tau^{\rm vis} = x\boldsymbol{p}_\tau, \qquad \boldsymbol{p}_\tau^{\rm invis} = (1-x)\boldsymbol{p}_\tau, \quad \text{and} \quad \boldsymbol{p}_\tau = \boldsymbol{p}_\tau^{\rm vis} + \boldsymbol{p}_\tau^{\rm invis}, \tag{21}$$

where x describes the fraction of the parent τ's momenta carried by the visible tau products and $0 \le x \le 1$. This approximation usually works well as long as the original τ momentum $\boldsymbol{p}_\tau$ is large compared with m_τ. To reconstruct $m_{\tau\tau}$ in $h\to\tau\tau$ events there is another assumption that the missing transverse momentum $\not{\boldsymbol{p}}_T$ consists of the two neutrinos from the two τ leptons, which can be written as

$$\not{\boldsymbol{p}}_T = c_1\boldsymbol{p}_{T,\tau_1}^{\rm vis} + c_2\boldsymbol{p}_{T,\tau_2}^{\rm vis}, \tag{22}$$

where $c_1 > 0$ and $c_2 > 0$. We have the relation $c_i = (1-x_i)/x_i$ for $i = 1, 2$.[4] In general, any missing momentum vector can be decomposed into the two vector in the transverse plane but not necessarily $c_1 > 0$ and $c_2 > 0$. So we only select such events to perform the collinear approximation. In this approximation, $\boldsymbol{p}_{\tau_1}^{\rm vis}, \boldsymbol{p}_{\tau_2}^{\rm vis}$ denote the two momenta of the visible decay products from the two τ leptons. Then, we can reconstruct the neutrino components by $\boldsymbol{p}_{\nu_i}^{\rm rec} = c_i\boldsymbol{p}_{\tau_i}^{\rm vis}$, or the original τ lepton momentum by $\boldsymbol{p}_{\tau_i}^{\rm rec} = \boldsymbol{p}_{\tau_i}^{\rm vis}/x_i$ and the invariant mass of the two τ leptons can be reconstructed as

$$m_{\rm col2}^2 = (p_{\tau_1}^{\rm rec} + p_{\tau_2}^{\rm rec})^2. \tag{23}$$

We can see also the relationship, $m_{\rm col2} = m_{\rm vis}/\sqrt{x_1x_2}$, where $m_{\rm vis}^2 = (p_{\tau_1}^{\rm vis} + p_{\tau_2}^{\rm vis})^2$ if we neglect the τ mass. This variable $m_{\rm col2}$ is the $m_{\rm coll}$ variable used in the ATLAS paper [71].

2. Collinear mass for one missing particle $m_{\rm col1}$

Although the above approach is ideal for reconstructing a $\tau\tau$ system, such as $h\to\tau\tau$ and $Z\to\tau\tau$ processes, relying on this variable does not make much sense for reconstructing $\tau\mu$ system where only one τ lepton exists. Thus, we consider another natural variable for detecting the $h\to\tau\mu$ process based on the straightforward assumption instead of Eq. (22), as

$$\not{\boldsymbol{p}}_T = c_1\boldsymbol{p}_{T,\tau}^{\rm vis} + c_\perp\hat{\boldsymbol{n}}_{T,\perp}, \tag{24}$$

where $\hat{\boldsymbol{n}}_{T,\perp}$ denotes a unit vector orthogonal to $\boldsymbol{p}_{T,\tau}^{\rm vis}$, or $\boldsymbol{p}_{T,\tau}^{\rm vis}\cdot\hat{\boldsymbol{n}}_{T,\perp} = 0$, in the transverse momentum plane. Although ideally the second term should vanish in $h\to\tau\mu$ signal events, since there are smearing effects due to, for example, the detector response and mismeasurements we introduce the term for successfully decompose any missing transverse momentum vector into the two transverse momentum vectors along with $\boldsymbol{p}_\tau^{\rm vis}$.

With the parameter c_1, we can reconstruct the neutrino momentum and the original τ lepton momentum as

[4]The missing transverse momentum is written as $\not{\boldsymbol{p}}_T$ and the transverse missing energy is $\not{E}_T = |\not{\boldsymbol{p}}_T|$.

TABLE III. Cut flow for m_{coll2} and m_{coll1} analyses. The number of the signal $h \to \tau_h\mu(\tau_R, \tau_L)$ and Z background are shown for $\mathcal{L} = 36.1$ fb^{-1}. Estimated upper bound for each signal region, $N^{95\%} = 1.65\sqrt{N_b}$ ($N_b = 2N_{Z\to\tau\tau}$), and the corresponding sensitivity values for BR($h \to \tau\mu$).

		$h \to \tau\mu_{(\text{BR}=1\%)}$				BR$^{95\%}$	
		τ_R	τ_L	$Z \to \tau_h\tau_\mu$	$N^{95\%}$	τ_R	τ_L
	σ at 13 TeV LHC for $\mathcal{L} = 36.1$ fb^{-1}	355 fb 12795		258 pb 9.31×10^6			
	baseline cuts	1979	1742	130147			
	$x_1 > 0$ and $x_2 > 0$	1672	1480	102536	747	0.45	0.50
m_{coll2}	$\lvert m_{\text{coll2}} - m_h\rvert < 25$ GeV	717	643	21473	342	0.48	0.53
	$\lvert m_{\text{coll2}} - m_h\rvert < 10$ GeV	344	304	7639	204	0.59	0.67
	$\lvert m_{\text{coll2}} - m_h\rvert < 5$ GeV	177	157	3776	143	0.81	0.91
	$c_1 > 0$	1765	1608	68602	610	0.34	0.38
m_{coll1}	$\lvert m_{\text{coll1}} - m_h\rvert < 25$ GeV	1626	1493	4023	148	0.091	0.099
	$\lvert m_{\text{coll1}} - m_h\rvert < 10$ GeV	1080	1008	639	58.9	0.055	0.059
	$\lvert m_{\text{coll1}} - m_h\rvert < 5$ GeV	617	577	216	34.2	0.056	0.059

$$\boldsymbol{p}^{\text{rec}}_{\nu_1} = c_1\boldsymbol{p}^{\text{vis}}_{\tau_1}, \quad \text{and} \quad \boldsymbol{p}^{\text{rec}}_{\tau_1} = \boldsymbol{p}^{\text{vis}}_{\tau_1}/x_1, \tag{25}$$

where we ideally expect $c_1 > 0$, or $0 < x_1 < 1$. Using this momentum we can compute reconstructed $m_{\tau\mu}$ as follows:

$$(m^{\text{rec}}_{\tau\mu})^2 = m^2_{\text{col1}} = (p^{\text{rec}}_{\tau_1} + p_\mu)^2. \tag{26}$$

We denote this variable as m_{col1} and more reasonable for reconstructing a $\tau\mu$ system based on the collinear approximation.[5]

In the following we show the difference between the analysis based on m_{col1} and m_{col2}. We first apply the baseline cut given in the previous section, inspired by the ATLAS analysis, and then apply the selection cuts to select only the reasonable events in each context of the collinear approximation. For the m_{col2} analysis, $c_1 > 0$ and $c_2 > 0$ should be required for the collinear approximation to be reasonable; however, it reduces too many signals. Therefore we instead require a weaker criteria $x_1 > 0$ and $x_2 > 0$, with which m_{col2} is computable. We found this is because the collinear approximation with the two missing particle assumption is not suitable for reconstructing a $\tau_h\mu$ system, and that is why the sensitivity based on it is worse. On the other hand, for the m_{col1} analysis, we apply $c_1 > 0$ as the corresponding condition but it is reasonable for reconstructing a $\tau_h\mu$ system. The number of events for the two signal samples $h \to \tau_R\mu_L$ (τ_R sample) and $h \to \tau_L\mu_R$ (τ_L sample), and $Z \to \tau\tau$ background sample after each step of the selection cuts are summarized in Table III. The numbers are for the integrated luminosity of 36.1 fb^{-1}. We only show the numbers for the cases τ_R and τ_L but the numbers for the nonpolarized case can be easily obtained by taking an average of the numbers in the two columns.

[5]CMS collaboration uses a similar variable m_{col} [73].

The m_{col2} and m_{col1} distributions at 36.1 fb^{-1} after the appropriate selection cuts are given in Fig. 3 in the left and right panels, respectively. The distributions for the signal samples τ_R (red), τ_L (blue) and the $Z \to \tau\tau$ sample (black dotted) are shown. We see that both variables m_{col2} and m_{col1} have a peak at $m_h = 125$ GeV. The m_{col1} peak is very sharp not only for the signal but also for the $Z \to \tau\tau$ BG, and we see a clear separation between the signal against the background distributions. On the other hand, m_{col2} distributions provide a broader peak and exhibit a significant overlap between the signal and background. Thus, we can reduce the background events by selecting the peak region keeping the signal evens, and more efficiently by m_{col1} than by m_{col2}.

We define the signal regions as $|\Delta m_{\text{col}i}| = |m_{\text{col}i} - m_h| \le \Delta m^{\text{th}}_{\text{col}i}$, and show the results for the three possible choices of $\Delta m^{\text{th}}_{\text{col}i} = 25$, 10, and 5 GeV. The numbers after selecting those signal regions are summarized in Table III. We observe that, by selecting m_{col2} region with 25 GeV width, the background can be reduced up to 0.23% while keeping the signal only about 5–6%. On the other hand, by selecting m_{col1} region with 25 GeV width, the background can be reduced down to 0.04% while keeping the signal about 12–13%. Therefore, using m_{col1} variable would provide a significant improved signal to background ratio. Another important observation is m_{col1} distribution provides a sharper peak, so in principle selecting a narrower signal region would improve the signal over background ratio, which one can explicitly see from Table III and only seen in m_{col1} analysis.

Note that our baseline selection cuts are inspired by the cuts given by the ATLAS analysis, and for the m_{col2} analysis the signal and $Z \to \tau\tau$ background numbers after requiring $x_1 > 0$ and $x_2 > 0$ are slightly larger but rather consistent with the numbers given in Table 5 in the ATLAS paper.

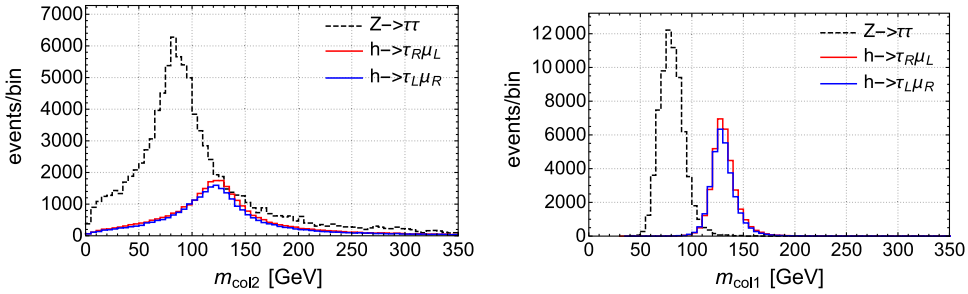

FIG. 3. The collinear mass $m_{\rm col2}$ (left) and $m_{\rm col1}$ (right) distributions for the signal samples τ_R and τ_L, and $Z \to \tau\tau$ background. The signal $m_{\rm col2}$ ($m_{\rm col1}$) distributions are scaled with a factor of 20.

We assume the total background contributions as the twice of the $Z \to \tau\tau$ background contributions following the same table, $N_b = 2N_{Z\to\tau\tau}$. We estimate the 95% C.L. upper bound of the signal number in a certain signal region as $N^{95\%} = 1.65\sqrt{N_b}$, where we employ a frequentist approach to obtain the one-side 95% C.L. interval. Then, from $N^{95\%}$ in each signal region, we estimate $\mathrm{BR}^{95\%}$, the 95% C.L. upper bound for the branching ratio $\mathrm{BR}(h \to \tau\mu)$, based on the expected signal numbers. Since the expected signal numbers depends on the signal assumptions τ_R or τ_L, or the τ polarization, the corresponding $\mathrm{BR}^{95\%}$ also depends on it. Note that we do not consider the systematic uncertainty to estimate the sensitivity, thus, a large signal over background ratio is important for those numbers to be reliable since the uncertainty effects become relatively small. Once one obtains the $\mathrm{BR}^{95\%}$, the corresponding $\bar{y}_{\tau\mu}^{95\%}$ can be calculated straightforwardly using Eq. (20).

Next, let us discuss the τ polarization effects. Already at the step at the baseline cuts, the signal efficiencies for τ_R and τ_L are different, and the τ_R sample survives more efficiently. The difference is about $\pm 6\%$ from the non-polarized case, which is understood by the effects of the jet p_T threshold. For the $m_{\rm col2}$ analysis, the difference is kept about $\pm 6\%$ after selecting the events with $x_1 > 0$ and $x_2 > 0$, and also the case after further selecting the $m_{\rm col2}$ peak region. Thus, interpreting the results based on $m_{\rm col2}$ analysis is sensitive to the polarization about 6%. On the other hand, for $m_{\rm col1}$ analysis the difference becomes diminished to $\pm 4.6\%$, and further weakened around the $m_{\rm col1}$ peak region to $\pm 3.3\%$. Final sensitivity is less sensitive when we use the $m_{\rm col1}$ but asymmetric behavior still exists.

Figure 4 shows our sensitivity results for the integrated luminosity of 36.1 fb^{-1} expressed in the $y_{\mu\tau} - y_{\tau\mu}$ plane, based on $m_{\rm col2}$ and $m_{\rm col1}$ analyses using only $\tau_h\mu$ modes. Unless the spin correlation effects are important, the contour of the exclusion boundary becomes an ellipse interpolating the values estimated by the two extreme cases τ_R and τ_L.

The green line shows the sensitivity based on the $m_{\rm col2}$ analysis, using the signal region of $\Delta m_{\rm col2}^{\rm th} = 25$ GeV, while the blue solid (dashed) line shows that based on the $m_{\rm col1}$ analysis for the $\Delta m_{\rm col1}^{\rm th} = 25$ GeV (5 GeV). By changing the analysis from $m_{\rm col2}$ to $m_{\rm col1}$, the sensitivity is significantly improved by a factor of 5 in terms of the constraints on the branching ratio. If we consider an even narrower signal region with $\Delta m_{\rm col1}^{\rm th} = 5$ and 10 GeV, the sensitivity is further improved by a factor of 10 compared with the $m_{\rm col2}$ analysis. It is thanks to the distinct peak shape of the $m_{\rm col1}$ distribution for the signal. Although we need to consider seriously whether the experimental smearing effects spoil this property or not, using $m_{\rm col1}$ would be advantageous since $m_{\rm col2}$ distribution does not have such a property. One can see that taking a narrower signal region does not improve the sensitivity for $m_{\rm col2}$ analysis.

Our estimate of the sensitivity by the $m_{\rm col2}$ analysis is close to the expected sensitivity in the non-VBF $\tau_h\mu$ mode of $\mathrm{BR}(h \to \tau\mu) = 0.57\%$ ($\bar{y}_{\tau\mu} = 0.0022$), which is shown in the red dashed line. Although we expect our sensitivity by a simple cut based analysis is worse than their sophisticated BDT analysis, these numbers coincide accidentally, which would be understood because we do not take the uncertainty into account. However, since the assumption of the setting for $m_{\rm col2}$ analysis and that for $m_{\rm col1}$ analysis are the same within our analysis, the

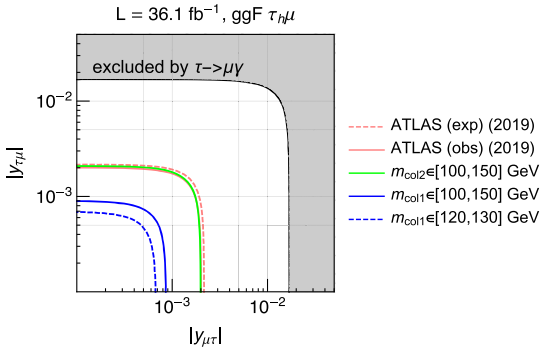

FIG. 4. Estimated upper bound on the flavor-violating Yukawa couplings $|y_{\tau\mu}|$,$|y_{\mu\tau}|$ using $h \to \tau_h\mu$ signals based on $m_{\rm col2}$ and $m_{\rm col1}$ analyses for integrated luminosity $\mathcal{L} = 36.1$ fb^{-1}. The ATLAS results are also shown for reference. The indirect limits from $\tau \to \mu\gamma$ searches [38,81] are indicated as the shaded region.

TABLE IV. Estimated sensitivity for the several assumed integrated luminosities $\mathcal{L} = 36.1$, 139, 1000, and 3000 fb^{-1}. The $N^{95\%}$ in the signal region, the corresponding sensitivities on the BR and $\bar{y}_{\mu\tau}$ are given. The two cases for $\Delta m_{\rm coll}^{\rm th} = 25$ and 5 GeV are shown. The unpolarized case $y_{\tau\mu} = y_{\mu\tau}$ is denoted as τ_0.

			BR$^{95\%}$ [$\times 10^{-4}$]			$\bar{y}_{\tau\mu}^{95\%}$ [$\times 10^{-4}$]		
$\Delta m_{\rm coll}^{\rm th}$	$\mathcal{L}$ [fb^{-1}]	$N^{95\%}$	τ_R	τ_0	τ_L	$y_{\mu\tau}$	$y_{\mu\tau} = y_{\tau\mu}$	$y_{\tau\mu}$
25 GeV	36.1	148	9.10	9.51	9.91	8.68	8.88	9.06
	139	290	4.64	4.85	5.05	6.20	6.34	6.47
	1000	779	1.73	1.81	1.88	3.79	3.87	3.95
	3000	1349	0.99	1.04	1.09	2.88	2.94	3.00
5 GeV	36.1	34.2	5.55	5.74	5.93	6.78	6.90	7.01
	139	67.1	2.83	2.93	3.02	4.84	4.92	5.01
	1000	180	1.06	1.09	1.13	2.96	3.01	3.06
	3000	312	0.61	0.63	0.65	2.25	2.28	2.32

improvement by using the $m_{\rm coll}$ for the analysis should persist.

The resulting sensitivity contours become not circles but ellipses in $(y_{\tau\mu}, y_{\mu\tau})$ plane when one includes the polarization effects appropriately.

Essentially their results are only rigorously correct along the line $y_{\tau\mu} = y_{\mu\tau}$ and the polarization effects would modify ±4–6% in the branching ratio, and ±2–3% in $(y_{\mu\tau}, y_{\tau\mu})$ plane. The current ATLAS bound based on the non-VBF $\tau_h\mu$ mode would also be modified.

According to the ATLAS analysis, combining all other modes of $h \to \tau\mu$ process improves the sensitivity about 35%, which gives the sensitivity down to BR$(h \to \tau\mu) = 0.37\%$ ($\bar{y}_{\tau\mu} = 0.0017$). The improvement factor of 5–10 is obtained only by changing the analysis strategy not by considering the other modes. Combining the sensitivity for the other modes applying $m_{\rm coll}$ analysis would improve the sensitivity further, and we expect it also 35% as a reference value, although we leave it for a future work since we need to perform a further study to confirm it.

D. Future prospect

1. Ultimate sensitivity

The sensitivity would scale with the integrated luminosity as proportional to $1/\sqrt{\mathcal{L}}$, since we employ the formula $N^{95\%} = 1.65\sqrt{N_b}$ for estimating it. The estimated upper limits on the branching ratio and the corresponding $\bar{y}_{\tau\mu}$ values for the several assumptions on the integrated luminosity $\mathcal{L}$ are summarized in Table IV. They are estimated by using the $\tau_h\mu$ channel only, and we would expect 35% improvements by combining all the other modes. As explained before, the τ_R sample gives a more stringent bound than the τ_L sample, and the effects are about ±4% in the branching ratio, and ±2% in the $\bar{y}_{\mu\tau}$ value.

This information is depicted in Fig. 5. We estimate that the upper bound $\bar{y}_{\tau\mu}^{95\%}$ at high luminosity LHC can be up to 3×10^{-4}, corresponding to BR$(h \to \tau\mu) \sim 10^{-4}$. Our result is in the same order of the result obtained in Ref. [43].

2. Sensitivity for the chirality structure

We would like to show how much sensitive to the chirality structure when we find the finite number of signals. For that we would like to show we can use the x_1 distribution, which naturally obtained along with computing the $m_{\rm coll}$ variable. To illustrate the procedure, let us take BR$(h \to \tau\mu) = 0.12\%$, corresponding to $\bar{y}_{\mu\tau} = 10^{-3}$ as a benchmark scenario, which is close to the best fit value for the recently reported excess by the ATLAS analysis with 138 fb^{-1} [72]. We consider the three cases keeping $\bar{y}_{\mu\tau} = 10^{-3}$: the purely τ_R case, the purely τ_L case, and the nonpolarized (τ_0) case, and for each case we assume that the expected number of events are exactly observed:

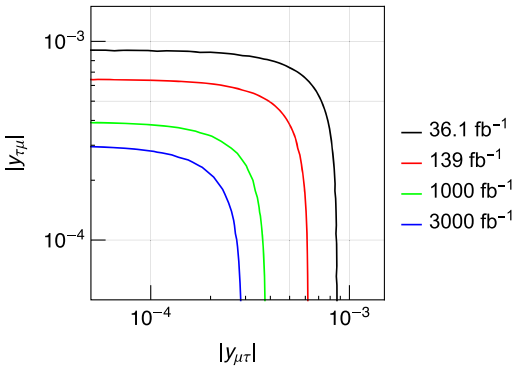

FIG. 5. Future prospects of the estimated sensitivity for the Yukawa couplings in $|y_{\mu\tau}|$,$|y_{\tau\mu}|$ plane based on the $m_{\rm coll}$ analysis with $\Delta m_{\rm coll}^{\rm th} = 25$ GeV using $h \to \tau_h\mu$ process. The expected results for the integrated luminosity of 36.1 fb^{-1}, 139 fb^{-1}, 1 ab^{-1}, and 3 ab^{-1} are shown.

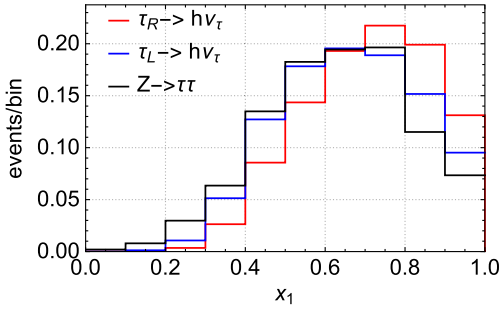

FIG. 6. Reconstructed x_1 distributions for the signal τ_R (red) and τ_L (blue), and for the $Z \to \tau\tau$ BG (black) in the signal region with $\Delta m_{\rm col1}^{\rm th} = 25$ GeV. All the distributions are normalized to unity.

$$(\hat{y}_{\mu\tau}, \hat{y}_{\tau\mu}) = \begin{cases} (10^{-3}, 0) & [\tau_R \text{ scenario}] \\ (0, 10^{-3}) & [\tau_L \text{ scenario}] \\ (7.1 \times 10^{-4}, 7.1 \times 10^{-4}) & [\tau_0 \text{ scenario}] \end{cases}. \tag{27}$$

In those three situations, we estimate how much we can constrain the parameters in $(y_{\mu\tau}, y_{\tau\mu})$ plane. As an illustration, the normalized reconstructed x_1 distributions for τ_R, τ_L, and $Z \to \tau\tau$ background are given in Fig. 6.

For simplicity we consider the simplest two bin analysis by further dividing the signal regions $\Delta m_{\rm col1}^{\rm th} = 25$ GeV based on the reconstructed x_1 values into two signal regions SR_1 and SR_2. We separate them as $\mathrm{SR} = \mathrm{SR}_1(x_1 < 0.6) + \mathrm{SR}_2(x_1 \geq 0.6)$, and the corresponding number of events found in the SRs we denote as $N = N(x_1 < 0.6) + N(x_1 \geq 0.6) = N_1 + N_2$. We denote the signal and background contributions found in SR_i $(i = 1, 2)$ as S_i and B_i, respectively.

We consider the three scenarios mentioned above and assume the observed number of events for the two signal regions are given by $N_{i,\rm obs} = S_i + B_i$, where we assume $B_i = 2B_{i,Z}$ as before. From the two numbers $N_{1,\rm obs}$ and $N_{2,\rm obs}$, we can fit simultaneously N_R and N_L. The estimated signal numbers for each scenario at the integrated luminosity of $\mathcal{L} = 36.1$ fb^{-1} are summarized in Table V. Based on the table, taking only statistical errors into account, a 1σ contour is obtained as an ellipse in the $(\Delta N_R, \Delta N_L)$ plane as follows:

$$\chi^2 = \left(\frac{r\Delta N_R + l\Delta N_L}{\sqrt{N_{1,\rm obs}}}\right)^2 + \left(\frac{(1-r)\Delta N_R + (1-l)\Delta N_L}{\sqrt{N_{2,\rm obs}}}\right)^2 \leq 2.3, \tag{28}$$

where ΔN_R and ΔN_L are the deviations from the best fit values, which are the assumed numbers for N_R and N_L in each scenario. Depending on the scenario, we take $(N_{1,\rm obs}, N_{2,\rm obs}) = \{(3435, 4807), (3443, 4791), (3451, 4776)\} \times (\mathcal{L}/36.1\ \text{fb}^{-1})$. The parameters r and l are the probabilities to fall into SR_1 for τ_R and τ_L, respectively. We obtain them as $r = 0.26$ and $l = 0.37$ from Table V. The contours described by the Yukawa parameters are obtained using the following relationship, with $N_R = 195.1$, $N_L = 179.2$,

$$\Delta N_R = N_R \left(\frac{\mathcal{L}}{36.1\ \text{fb}^{-1}}\right) \frac{|y_{\mu\tau}|^2 - |\hat{y}_{\mu\tau}|^2}{10^{-6}}, \tag{29}$$

$$\Delta N_L = N_L \left(\frac{\mathcal{L}}{36.1\ \text{fb}^{-1}}\right) \frac{|y_{\tau\mu}|^2 - |\hat{y}_{\tau\mu}|^2}{10^{-6}}. \tag{30}$$

The expected 1σ contours for $\Delta m_{\rm col1}^{\rm th} = 25$ GeV are shown in Fig. 7. We show the results for the integrated luminosity at 36.1, 139, 1000, and 3000 fb^{-1}. For the conservative choice for the signal region width of $\Delta m_{\rm col1}^{\rm th} = 25$ GeV, the chirality structure would become sensitive after 1000 fb^{-1}. For example, extreme cases between the τ_R scenario and τ_L scenario can be distinguished at 2.3σ (4.4σ) at 1000 (3000) fb^{-1}. The τ_R scenario and τ_0 scenario can be distinguished at 1.9σ at 3000 fb^{-1}. The reason that the sensitivity is not strong is due to the relatively large background contribution, which dilutes the sensitivity to the chirality of the system.

Further, we show the expected 1σ contours for $\Delta m_{\rm col1}^{\rm th} = 5$ GeV in Fig. 8 for the integrated luminosity

TABLE V. Number of events in the SR_1 $(x_1 < 0.6)$ and SR_2 $(x_1 \geq 0.6)$ for $\mathcal{L} = 36.1$ fb^{-1}. The results of the two possible choices for the width of the signal region $\Delta m_{\rm col1}^{\rm th} = 25$ and 5 GeV are shown.

		$N_{i,\rm BR=0.12\%}$			N_i/N			$N_{i,\rm obs}$ for each scenario		
$\Delta m_{\rm col1}^{\rm th}$	SR	τ_R	τ_L	$Z \to \tau\tau$	τ_R	τ_L	$Z \to \tau\tau$	τ_R	τ_0	τ_L
25 GeV	SR_1	50.6	66.1	1692	0.26	0.37	0.42	3436	3443	3451
	SR_2	144.5	113.1	2331	0.74	0.63	0.58	4807	4791	4776
	total	195.1	179.2	4023	1	1	1	8243	8234	8227
5 GeV	SR_1	17.8	25.6	136	0.24	0.37	0.37	289.8	293.7	297.6
	SR_2	56.2	43.6	80	0.76	0.63	0.63	216.2	209.9	203.6
	total	74.0	69.2	216.0	1	1	1	506	503.6	501.2

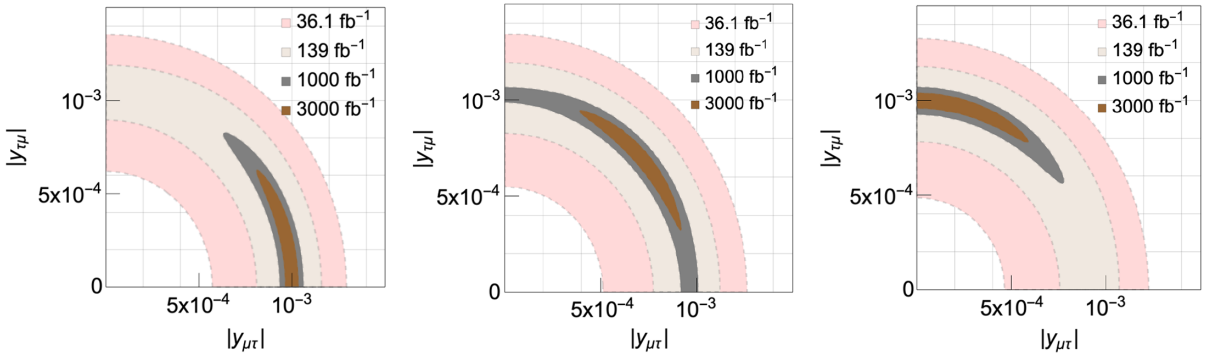

FIG. 7. Estimated sensitivity for the chirality structure in $h \to \tau\mu$ process using the signal region with $\Delta m_{\mathrm{col1}}^{\mathrm{th}} = 25$ GeV. The results for the three types of benchmark points predicting $\mathrm{BR}(h \to \tau\mu) = 0.12\%$, τ_R scenario (left), τ_0 scenario (center), and τ_L scenario (right) are shown. The 1σ contours for the integrated luminosity at 36.1, 139, 1000, and 3000 fb^{-1} are shown.

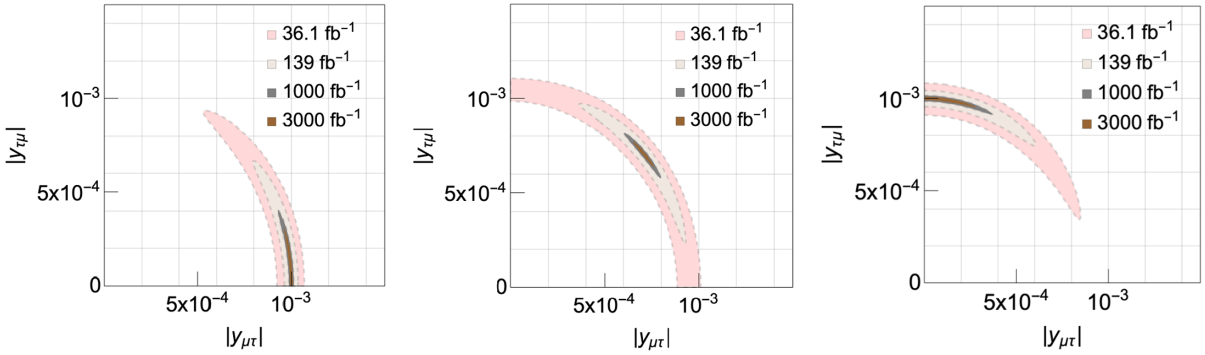

FIG. 8. Estimated sensitivity for the chirality structure in $h \to \tau\mu$ process using the signal region with $\Delta m_{\mathrm{col1}}^{\mathrm{th}} = 5$ GeV. The results for the three types of benchmark points predicting $\mathrm{BR}(h \to \tau\mu) = 0.12\%$, τ_R scenario (left), τ_0 scenario (center), and τ_L scenario (right) are shown. The 1σ contours for the integrated luminosity at 36.1, 139, 1000, and 3000 fb^{-1} are shown.

at 36.1, 139, 1000, and 3000 fb^{-1}. By taking the narrower signal region width of $\Delta m_{\mathrm{col1}}^{\mathrm{th}} = 5$ GeV, the signal over background ratio would become improved from about $1/40$ to about $1/6$, and the chirality structure would be distinguishable already at 139 fb^{-1}. For example, an extreme case τ_R scenario would be distinguished from the non-polarized scenario (τ_L scenario) at 2.1σ (4.8σ) level at 139 fb^{-1}. Note that as we do not take the systematic uncertainty into account, these numbers should be rather optimistic and taken as reference values. Nevertheless, we expect that accumulating more data would make such a sensitivity achievable and more detailed experimental study is desirable.

V. CONCLUSION

The Higgs LFV process is a smoking gun signature of new physics beyond the SM. The chirality structure of the process is important information to discriminate the models, but it is not often discussed in detail. Most of the experimental results reported basically assume no chirality preference. In this paper, we consider how much we can probe the chirality structure in the $h \to \mu\tau$ process at the LHC.

We first discuss that to reconstruct the $h \to \tau\mu$ process, the collinear approximation with one missing particle assumption would be more effective than that with two missing particle assumption. Thus, we compare the analysis with m_{col1} variable and that with m_{col2} variable. We have shown that using the m_{col1} variable would improve the signal over background ratio more easily than using the m_{col2} variable, since the m_{col1} distribution exhibits a sharp peak structure at the Higgs mass for the $h \to \tau\mu$ signal process. We estimated the ultimate sensitivity of this process based on the m_{col1} analysis. We then showed that the τ polarization affects the acceptance of the signature due to the jet p_T threshold. Consequently, the current search results should be altered by the polarization effects. We estimate the size of the effects and found that it is about at $\pm 4\%$ level in terms of the $\mathrm{BR}(h \to \tau\mu)$. As a result the exclusion contour should become in general not a circle but an ellipse, where in general we have stronger constraints on $y_{\mu\tau}$ that governs the $h \to \tau_R\mu_L$ contributions.

Inspired by the recent 2σ level excess reported in this process, we discuss whether the chirality structure is distinguishable or not, by considering the three benchmark scenarios with different chirality structures. We utilize the reconstructed x_1 distributions for this purpose

and demonstrate the simplest two bin analysis to obtain the 1σ contours in two-dimensional parameter space for the several assumptions of the integrated luminosities. Note that for this analysis, adopting m_{col1} analysis is important since appropriately estimating the invisible momentum of the τ decay is required to reconstruct the x_1 variable. As a result, we found that the two extreme cases of the chirality structures, the τ_R scenario and τ_L scenario, would be distinguishable at 1000 fb^{-1} at 2σ level. We also show that taking a narrower signal region increases the signal over background and enhances the sensitivity. For this setup, we found the two extreme cases would be distinguishable already at 139 fb^{-1} although a dedicated experimental study would be required to confirm the feasibility.

Once we have a sensitivity for the chirality structure of the off-diagonal elements $y_{\mu\tau}$ and $y_{\tau\mu}$ separately, we would be able to distinguish the new physics models. For example, there are models predicting the following relation [77] in the 2HDM,

$$\mathcal{L}_{\mathrm{LFV}} \propto \frac{m_\tau}{v}\tau_L\mu_R + \frac{m_\mu}{v}\mu_L\tau_R + \mathrm{H.c.} \tag{31}$$

Since $m_\tau \gg m_\mu$, we can discuss whether these types of models are preferred or excluded.

Another interesting study to be done in the 2HDM framework would be to discuss the correlation between the HLFV and the chirality structure of the heavy resonances. The off-diagonal $\xi_{\tau\mu}$ component contributes to the $h \to \tau\mu$ process and the couplings to the heavy resonances. Thus, the existence of the HLFV process naturally predicts the existence of the LFV coupling to the heavy resonances, which induces the LFV heavy resonance decay, for example, the heavy Higgs decay $H \to \tau\mu$. Following a similar analysis demonstrated in this paper, we would also be able to analyze the chirality structure of the Yukawa couplings to the heavy Higgses. We leave this analysis for a future work.

ACKNOWLEDGMENTS

This work was supported, in part, by the JSPS KAKENHI Grant, the Grant-in-Aid for Scientific Research A, No. 20H00160 (S. K., M. A.). M. T. is supported by the Fundamental Research Funds for the Central Universities, the One Hundred Talent Program of Sun Yat-sen University, China, and by the JSPS KAKENHI Grant, the Grant-in-Aid for Scientific Research C, Grant No. 18K03611.

[1] S. Chatrchyan *et al.* (CMS Collaboration), Phys. Lett. B **716**, 30 (2012).
[2] G. Aad *et al.* (ATLAS Collaboration), Phys. Lett. B **716**, 1 (2012).
[3] J. L. Diaz-Cruz and J. J. Toscano, Phys. Rev. D **62**, 116005 (2000).
[4] S. Kanemura, T. Ota, and K. Tsumura, Phys. Rev. D **73**, 016006 (2006).
[5] A. Crivellin, G. D'Ambrosio, and J. Heeck, Phys. Rev. Lett. **114**, 151801 (2015).
[6] A. Crivellin, J. Heeck, and P. Stoffer, Phys. Rev. Lett. **116**, 081801 (2016).
[7] F. J. Botella, G. C. Branco, M. Nebot, and M. N. Rebelo, Eur. Phys. J. C **76**, 161 (2016).
[8] Y. Omura, E. Senaha, and K. Tobe, Phys. Rev. D **94**, 055019 (2016).
[9] M. Sher and K. Thrasher, Phys. Rev. D **93**, 055021 (2016).
[10] J. Herrero-García, T. Ohlsson, S. Riad, and J. Wirén, J. High Energy Phys. 04 (2017) 130.
[11] W.-S. Hou, R. Jain, C. Kao, M. Kohda, B. McCoy, and A. Soni, Phys. Lett. B **795**, 371 (2019).
[12] T. Nomura and K. Yagyu, J. High Energy Phys. 10 (2019) 105.
[13] A. Vicente, Front. Phys. **7**, 174 (2019).
[14] W.-S. Hou and G. Kumar, Phys. Rev. D **101**, 095017 (2020).
[15] A. Pilaftsis, Phys. Lett. B **285**, 68 (1992).
[16] E. Arganda, A. M. Curiel, M. J. Herrero, and D. Temes, Phys. Rev. D **71**, 035011 (2005).
[17] E. Arganda, M. J. Herrero, X. Marcano, and C. Weiland, Phys. Rev. D **91**, 015001 (2015).
[18] M. Aoki, S. Kanemura, K. Sakurai, and H. Sugiyama, Phys. Lett. B **763**, 352 (2016).
[19] E. Arganda, M. J. Herrero, X. Marcano, R. Morales, and A. Szynkman, Phys. Rev. D **95**, 095029 (2017).
[20] N. H. Thao, L. T. Hue, H. T. Hung, and N. T. Xuan, Nucl. Phys. **B921**, 159 (2017).
[21] X. Marcano and R. A. Morales, Front. Phys. **7**, 228 (2020).
[22] J. L. Diaz-Cruz, J. High Energy Phys. 05 (2003) 036.
[23] A. Brignole and A. Rossi, Phys. Lett. B **566**, 217 (2003).
[24] S. Kanemura, K. Matsuda, T. Ota, T. Shindou, E. Takasugi, and K. Tsumura, Phys. Lett. B **599**, 83 (2004).
[25] A. Crivellin, Phys. Rev. D **83**, 056001 (2011).
[26] P. T. Giang, L. T. Hue, D. T. Huong, and H. N. Long, Nucl. Phys. **B864**, 85 (2012).
[27] A. Arhrib, Y. Cheng, and O. C. W. Kong, Europhys. Lett. **101**, 31003 (2013).
[28] M. Arana-Catania, E. Arganda, and M. J. Herrero, J. High Energy Phys. 09 (2013) 160; 10 (2015) 192.
[29] A. Abada, M. E. Krauss, W. Porod, F. Staub, A. Vicente, and C. Weiland, J. High Energy Phys. 11 (2014) 048.
[30] E. Arganda, M. J. Herrero, X. Marcano, and C. Weiland, Phys. Rev. D **93**, 055010 (2016).

[31] E. Arganda, M. J. Herrero, R. Morales, and A. Szynkman, J. High Energy Phys. 03 (2016) 055.
[32] H.-B. Zhang, T.-F. Feng, S.-M. Zhao, Y.-L. Yan, and F. Sun, Chin. Phys. C **41**, 043106 (2017).
[33] S. Fathy, T. Ibrahim, A. Itani, and P. Nath, Phys. Rev. D **94**, 115029 (2016).
[34] M. E. Gomez, S. Heinemeyer, and M. Rehman, J. Part. Phys. **1**, 30 (2017).
[35] U. Cotti, M. Pineda, and G. Tavares-Velasco, arXiv:hep-ph/0501162.
[36] A. Goudelis, O. Lebedev, and J.-h. Park, Phys. Lett. B **707**, 369 (2012).
[37] G. Blankenburg, J. Ellis, and G. Isidori, Phys. Lett. B **712**, 386 (2012).
[38] R. Harnik, J. Kopp, and J. Zupan, J. High Energy Phys. 03 (2013) 026.
[39] A. Celis, V. Cirigliano, and E. Passemar, Phys. Rev. D **89**, 013008 (2014).
[40] S. Banerjee, B. Bhattacherjee, M. Mitra, and M. Spannowsky, J. High Energy Phys. 07 (2016) 059.
[41] I. Chakraborty, S. Mondal, and B. Mukhopadhyaya, Phys. Rev. D **96**, 115020 (2017).
[42] T. Davidek and L. Fiorini, Front. Phys. **8**, 149 (2020).
[43] R. K. Barman, P. S. B. Dev, and A. Thapa, arXiv:2210.16287.
[44] S. Davidson and P. Verdier, Phys. Rev. D **86**, 111701 (2012).
[45] S. Bressler, A. Dery, and A. Efrati, Phys. Rev. D **90**, 015025 (2014).
[46] A. Dery, A. Efrati, Y. Nir, Y. Soreq, and V. Susič, Phys. Rev. D **90**, 115022 (2014).
[47] J. Heeck, M. Holthausen, W. Rodejohann, and Y. Shimizu, Nucl. Phys. **B896**, 281 (2015).
[48] L. de Lima, C. S. Machado, R. D. Matheus, and L. A. F. do Prado, J. High Energy Phys. 11 (2015) 074.
[49] X.-G. He, J. Tandean, and Y.-J. Zheng, J. High Energy Phys. 09 (2015) 093.
[50] K. Cheung, W.-Y. Keung, and P.-Y. Tseng, Phys. Rev. D **93**, 015010 (2016).
[51] S. Baek and K. Nishiwaki, Phys. Rev. D **93**, 015002 (2016).
[52] S. Baek and Z.-F. Kang, J. High Energy Phys. 03 (2016) 106.
[53] L. T. Hue, H. N. Long, T. T. Thuc, and T. Phong Nguyen, Nucl. Phys. **B907**, 37 (2016).
[54] C.-F. Chang, C.-H. V. Chang, C. S. Nugroho, and T.-C. Yuan, Nucl. Phys. **B910**, 293 (2016).
[55] I. Chakraborty, A. Datta, and A. Kundu, J. Phys. G **43**, 125001 (2016).
[56] A. Lami and P. Roig, Phys. Rev. D **94**, 056001 (2016).
[57] W. Altmannshofer, M. Carena, and A. Crivellin, Phys. Rev. D **94**, 095026 (2016).
[58] J. Herrero-Garcia, N. Rius, and A. Santamaria, J. High Energy Phys. 11 (2016) 084.
[59] A. Hayreter, X.-G. He, and G. Valencia, Phys. Rev. D **94**, 075002 (2016).
[60] R. M. Fonseca and M. Hirsch, Phys. Rev. D **94**, 115003 (2016).
[61] Q. Qin, Q. Li, C.-D. Lü, F.-S. Yu, and S.-H. Zhou, Eur. Phys. J. C **78**, 835 (2018).
[62] T. T. Hong, H. T. Hung, H. H. Phuong, L. T. T. Phuong, and L. T. Hue, Prog. Theor. Exp. Phys. **2020**, 043B03 (2020).
[63] T. P. Nguyen, T. T. Thuc, D. T. Si, T. T. Hong, and L. T. Hue, Prog. Theor. Exp. Phys. **2022**, 023B01 (2022).
[64] H. T. Hung, N. T. Tham, T. T. Hieu, and N. T. T. Hang, Prog. Theor. Exp. Phys. **2021**, 083B01 (2021).
[65] Z.-N. Zhang, H.-B. Zhang, J.-L. Yang, S.-M. Zhao, and T.-F. Feng, Phys. Rev. D **103**, 115015 (2021).
[66] M. Zeleny-Mora, J. L. Díaz-Cruz, and O. Félix-Beltrán, arXiv:2112.08412.
[67] R. S. Hundi, Eur. Phys. J. C **82**, 505 (2022).
[68] H. T. Hung, D. T. Binh, and H. V. Quyet, Chin. Phys. C **46**, 123104 (2022).
[69] A. Abada, J. Kriewald, E. Pinsard, S. Rosauro-Alcaraz, and A. M. Teixeira, arXiv:2207.10109.
[70] A. M. Baldini *et al.* (MEG Collaboration), Eur. Phys. J. C **76**, 434 (2016).
[71] G. Aad *et al.* (ATLAS Collaboration), Phys. Lett. B **800**, 135069 (2020).
[72] ATLAS Collaboration Collaboration, Report No. ATLAS-CONF-2022-060, 2022, 10.48550/arXiv.2302.05225.
[73] A. M. Sirunyan *et al.* (CMS Collaboration), Phys. Rev. D **104**, 032013 (2021).
[74] W. Altmannshofer *et al.* (Belle-II Collaboration), Prog. Theor. Exp. Phys. **2019**, 123C01 (2019); **2020**, 029201 (2020).
[75] R. D. Peccei, T. T. Wu, and T. Yanagida, Phys. Lett. B **172**, 435 (1986).
[76] C.-R. Chen, P. H. Frampton, F. Takahashi, and T. T. Yanagida, J. High Energy Phys. 06 (2010) 059.
[77] C.-W. Chiang, H. Fukuda, M. Takeuchi, and T. T. Yanagida, J. High Energy Phys. 11 (2015) 057.
[78] C.-W. Chiang, H. Fukuda, M. Takeuchi, and T. T. Yanagida, Phys. Rev. D **97**, 035015 (2018).
[79] C.-W. Chiang, M. Takeuchi, P.-Y. Tseng, and T. T. Yanagida, Phys. Rev. D **98**, 095020 (2018).
[80] T. Li and M. A. Schmidt, Phys. Rev. D **99**, 055038 (2019).
[81] B. Aubert *et al.* (*BABAR* Collaboration), Phys. Rev. Lett. **104**, 021802 (2010).
[82] B. Abi, T. Albahri, S. Al-Kilani, D. Allspach*et al.*, Phys. Rev. Lett. **126**, 141801 (2021).
[83] G. W. Bennett, B. Bousquet, H. N. Brown, G. Bunce, R. M. Carey, P. Cushman*et al.*, Phys. Rev. D **80**, 052008 (2009).
[84] A. Collaboration, Phys. Lett. B **485**, 37 (2000).
[85] B. Collaboration, Phys. Lett. B **551**, 16 (2003).
[86] S. Kanemura, Y. Kuno, M. Kuze, and T. Ota, Phys. Lett. B **607**, 165 (2005).
[87] M. Takeuchi, Y. Uesaka, and M. Yamanaka, Phys. Lett. B **772**, 279 (2017).
[88] Y. Kiyo, M. Takeuchi, Y. Uesaka, and M. Yamanaka, J. High Energy Phys. 04 (2022) 044.
[89] K. Hayasaka *et al.*, Phys. Lett. B **687**, 139 (2010).
[90] A. Dedes, W. Materkowska, M. Paraskevas, J. Rosiek, and K. Suxho, J. High Energy Phys. 06 (2017) 143.
[91] B. Grzadkowski, M. Iskrzynski, M. Misiak, and J. Rosiek, J. High Energy Phys. 10 (2010) 085.
[92] R. Primulando and P. Uttayarat, J. High Energy Phys. 05 (2017) 055.

[93] E. Arganda, X. Marcano, N. I. Mileo, R. A. Morales, and A. Szynkman, Eur. Phys. J. C **79**, 738 (2019).
[94] R. Primulando, J. Julio, and P. Uttayarat, Phys. Rev. D **101**, 055021 (2020).
[95] W.-s. Hou, R. Jain, and C. Kao, arXiv:2202.04336.
[96] B. K. Bullock, K. Hagiwara, and A. D. Martin, Nucl. Phys. **B395**, 499 (1993).
[97] K. Hagiwara, T. Li, K. Mawatari, and J. Nakamura, Eur. Phys. J. C **73**, 2489 (2013).
[98] K. Hagiwara, A. D. Martin, and D. Zeppenfeld, Phys. Lett. B **235**, 198 (1990).
[99] J. Alwall, R. Frederix, S. Frixione, V. Hirschi, F. Maltoni, O. Mattelaer, H. S. Shao, T. Stelzer, P. Torrielli, and M. Zaro, J. High Energy Phys. 07 (2014) 079.
[100] T. Sjöstrand, S. Ask, J. R. Christiansen, R. Corke, N. Desai, P. Ilten, S. Mrenna, S. Prestel, C. O. Rasmussen, and P. Z. Skands, Comput. Phys. Commun. **191**, 159 (2015).
[101] J. de Favereau, C. Delaere, P. Demin, A. Giammanco, V. Lemaître, A. Mertens, and M. Selvaggi (DELPHES 3 Collaboration), J. High Energy Phys. 02 (2014) 057.
[102] S. Dittmaier *et al.* (LHC Higgs Cross Section Working Group), Report No. CERN-2011-002, 2011, 10.5170/CERN-2011-002.
[103] S. Dittmaier *et al.*, Report No. CERN-2012-002, 2012, 10.5170/CERN-2012-002.
[104] J. R. Andersen *et al.* (LHC Higgs Cross Section Working Group), Report No. CERN-2013-004, 2013, 10.5170/CERN-2013-004.
[105] D. de Florian *et al.* (LHC Higgs Cross Section Working Group), Report No. CYRM-2017-002, 2016, 10.23731/CYRM-2017-002.
[106] A. Elagin, P. Murat, A. Pranko, and A. Safonov, Nucl. Instrum. Methods Phys. Res., Sect. A **654**, 481 (2011).